



Electronic structure and resonant inelastic x-ray scattering in osmates. II. Pyrochlore $\text{Cd}_2\text{Os}_2\text{O}_7$ V. N. Antonov ¹, D. A. Kukusta,^{1,2} and L. V. Bekenov¹¹*G. V. Kurdyumov Institute for Metal Physics of the National Academy of Sciences of Ukraine, 36 Academician Vernadsky Boulevard, UA-03142 Kyiv, Ukraine*²*Max Planck Institute for Solid State Research, Heisenbergstrasse 1, 70569 Stuttgart, Germany* (Received 22 September 2021; revised 4 February 2022; accepted 30 March 2022; published 21 April 2022)

We have investigated the electronic and magnetic properties of the pyrochlore osmate $\text{Cd}_2\text{Os}_2\text{O}_7$ within density functional theory using the generalized gradient approximation with taking into account strong Coulomb correlations in the framework of the fully relativistic spin-polarized Dirac linear muffin-tin orbital band-structure method. $\text{Cd}_2\text{Os}_2\text{O}_7$ is a Mott insulator with all-in-all-out magnetic order. The optical spectra, x-ray absorption spectra, and x-ray magnetic circular dichroism at the Os $L_{2,3}$ edges in the pyrochlore osmate $\text{Cd}_2\text{Os}_2\text{O}_7$ have been investigated theoretically from first principles. The calculated results are in good agreement with experimental data. We have also investigated theoretically the resonant inelastic x-ray scattering (RIXS) spectrum at the Os L_3 edge. The experimentally measured RIXS spectrum of $\text{Cd}_2\text{Os}_2\text{O}_7$ in addition to the elastic scattering peak at 0 eV possesses a sharp feature at 0.9 eV corresponding to transitions within the Os t_{2g} levels, a strong intense peak at around 4.5 eV which is from $t_{2g} \rightarrow e_g$ transitions, and a wide structure stretching from 5.5 eV to 15 eV that corresponds to ligand-to-metal charge transfer excitations.

DOI: [10.1103/PhysRevB.105.155145](https://doi.org/10.1103/PhysRevB.105.155145)**I. INTRODUCTION**

The pyrochlore $\text{Cd}_2\text{Os}_2\text{O}_7$, which was first characterized by Sleight *et al.* [1], shows a peculiar metal-insulator transition (MIT) at 227 K with magnetic ordering in a frustrated pyrochlore lattice at the same temperature. Mandrus *et al.* [2] showed that this MIT is a continuous, second-order transition accompanied by magnetic order. Yamaura *et al.* [3] proposed an all-in-all-out (AIAO) magnetic structure for $\text{Cd}_2\text{Os}_2\text{O}_7$, based upon resonant elastic x-ray scattering data. It was supported by many-body quantum-chemical calculations [4] and neutron powder diffraction (NPD) measurements [5]. Recent high-resolution resonant inelastic x-ray scattering (RIXS) measurements provided by Vale *et al.* [6] also confirm that the magnetic ground state of $\text{Cd}_2\text{Os}_2\text{O}_7$ is AIAO. Such magnetic configuration has also been found for some isostructural rare-earth pyrochlore compounds $R_2\text{Ir}_2\text{O}_7$ ($R = \text{Y}, \text{Nd}, \text{Sm}, \text{and Eu}$) [7–9]. Recently Wang *et al.* discovered experimentally that the Néel temperature in $\text{Cd}_2\text{Os}_2\text{O}_7$ is continuously suppressed with applied hydrostatic pressure, going to zero temperature at 36 GPa [10].

A detailed analysis of the x-ray diffraction (XRD) data did not produce any indications for structural changes at $T < T_{MIT}$ [11]. These observations allow us to conclude that the metal-insulator transition in $\text{Cd}_2\text{Os}_2\text{O}_7$ is driven solely by electronic processes without noticeable indications for involvement of the lattice. Another important fact pertaining to the nature of the insulating state is the continuous development of the energy gap in the optical conductivity $\sigma_{1xx}(\omega)$ [12]. Besides, the gap edge has a distinct $\sigma_{1xx}(\omega) \sim \omega^{1/2}$ dependence, as is expected for a Slater transition. This finding is important because the $\omega^{1/2}$ dependence is distinct from

the $\omega^{3/2}$ dependence observed in the Hubbard limit [13]. The revelation of the noncollinear AIAO spin arrangement ruled out the Slater mechanism suggested earlier by Mandrus *et al.* [2]. Some authors argued that the MIT in $\text{Cd}_2\text{Os}_2\text{O}_7$ is induced by the variation of Fermi surface topology (the Lifshitz transition) [14–16].

In the present work we report a detailed theoretical investigation of the electronic structure and RIXS spectra of $\text{Cd}_2\text{Os}_2\text{O}_7$. This paper is the second in a series of two papers. The first paper [17] is devoted to a theoretical investigation of the RIXS spectra of perovskite NaOsO_3 . The RIXS spectrum in $\text{Cd}_2\text{Os}_2\text{O}_7$ was measured by Vale *et al.* [6] in the 0–1 eV energy interval. Calder *et al.* [5] presented the RIXS spectra within a wider energy range up to 8 eV. We also investigated theoretically the optical spectra of $\text{Cd}_2\text{Os}_2\text{O}_7$ as well as the x-ray absorption spectra (XAS) and x-ray magnetic circular dichroism (XMCD) at the Os $L_{2,3}$ edges. Matsuda *et al.* [18] measured the XAS and XMCD spectra at the Os $L_{2,3}$ edges. The optical absorption spectra of $\text{Cd}_2\text{Os}_2\text{O}_7$ were investigated by Padilla *et al.* [12] and Sohn *et al.* [15]. The electronic structure of $\text{Cd}_2\text{Os}_2\text{O}_7$ was studied by several authors [2,6,15,19–23] using different approximations. The energy band structure of $\text{Cd}_2\text{Os}_2\text{O}_7$ in this paper is calculated within the *ab initio* approach by applying the generalized gradient approximation (GGA) using the fully relativistic spin-polarized Dirac linear muffin-tin orbital (LMTO) band-structure method with taking into account strong electron-electron correlations (within the GGA+ U approach).

This paper II is organized as follows. The crystal structure of $\text{Cd}_2\text{Os}_2\text{O}_7$ and computational details are presented in Sec. II. Section III presents the electronic and magnetic

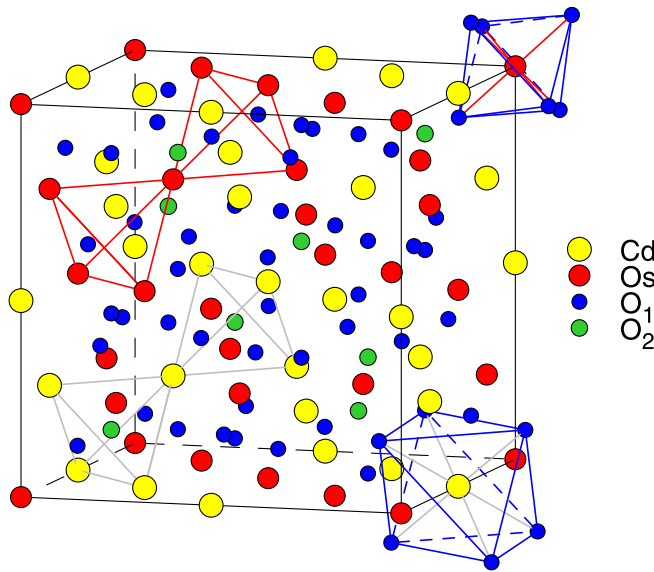


FIG. 1. The crystal structure of the pyrochlore osmate $\text{Cd}_2\text{Os}_2\text{O}_7$ (the space group is $Fd\bar{3}m$, No. 227). Red spheres represent osmium atoms, blue and green spheres show oxygen atoms, yellow spheres represent Cd atoms.

structures of $\text{Cd}_2\text{Os}_2\text{O}_7$. In Sec. IV the theoretical investigations of the RIXS spectrum of $\text{Cd}_2\text{Os}_2\text{O}_7$ at the Os L_3 edge are presented, and the theoretical results are compared with experimental measurements. Section V is devoted to the XAS and XMCD spectra of the $\text{Cd}_2\text{Os}_2\text{O}_7$ compound at the Os $L_{2,3}$ edges. Finally, the results are summarized in Sec. VI.

II. COMPUTATIONAL DETAILS

A. Crystal structure

$\text{Cd}_2\text{Os}_2\text{O}_7$ crystallizes in the cubic pyrochlore structure (space group $Fd\bar{3}m$) with OsO_6 octahedra connected by their vertices with interpenetrating Cd-O framework [24] (Fig. 1). The Cd atoms are situated at the $16d$ position (0.5, 0.5, 0.5), Os at the $16c$ position (0, 0, 0), O_1 at the $48f$ ($x, 0.125, 0.125$), and O_2 at the $8a$ (0.375, 0.375, 0.375) positions. In each unit cell there are 8 formula units. Only two parameters in this structure, namely the lattice constant a and the x coordinate associated with the O_1 site, are adjustable. The positional parameter x provides a measure of the distortion of the OsO_6 octahedra, with $x_c = 5/16 = 0.3125$ corresponding to ideal undistorted octahedra. For $x > 5/16$ the OsO_6 octahedra become trigonally compressed, while for $x < 5/16$ they become trigonally elongated. $\text{Cd}_2\text{Os}_2\text{O}_7$ has $x = 0.319$ [2] larger than the value for ideal OsO_6 octahedra x_c , indicating that a compressive trigonal distortion is present with the Os-O-Os angle reduced from ideal $\sim 141^\circ$.

The Os atoms have six O_1 atoms as nearest neighbors (at 1.928 Å distance), six O_1 atoms at 3.7053 Å distance, and six O_2 atoms at 4.212 Å distance, while for Cd there are six O_1 atoms at 2.5705 Å distance, twelve O_1 atoms at 4.0767 Å distance, and two O_2 atoms at 2.1997 Å distance.

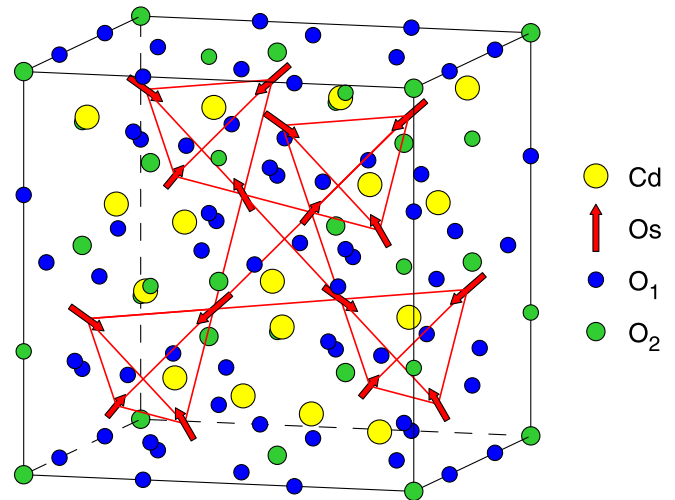


FIG. 2. The spin AIAO magnetic structure in $\text{Cd}_2\text{Os}_2\text{O}_7$.

B. Calculation details

The details of the computational method are described in the first paper of this series [17] and here we only mention several aspects. The calculations were performed for the experimentally observed lattice constant $a = 10.1598$ Å [2]. The exchange-correlation functional of a GGA-type was used in the version of Perdew, Burke, and Ernzerhof (PBE) [25]. The Brillouin zone (BZ) integration was performed using the improved tetrahedron method [26]. The basis consisted of Os and Cd s , p , d , and f ; and O s , p , and d LMTOs.

The finite lifetime of a core hole was accounted for by folding the spectra with a Lorentzian. The widths of core levels were taken from Ref. [27]. The finite experimental resolution of the spectrometer used for the measurements of the XAS and XMCD spectra was accounted for by a Gaussian of 0.6 eV width.

Although it is widely believed that the d - d excitations show only a small momentum transfer vector \mathbf{Q} dependence in transition metal oxides [28], we choose in our RIXS calculations the vector \mathbf{Q} used in the corresponding RIXS measurements, namely, $\mathbf{Q} = (2.5, 8.8, 8.8)$ [5].

III. ELECTRONIC AND MAGNETIC STRUCTURES

All possible magnetic structures in the pyrochlore compounds with space group $Fd\bar{3}m$ can be classified by finding the magnetic co-representation for the tetrahedron group: $c\Gamma_{\text{mag}} = c\Gamma_{3+} + c\Gamma_{5+} + c\Gamma_{7+} + c\Gamma_{9+}$ [3,29,30]. We found that the one-dimensional $c\Gamma_{3+}$ representation with the AIAO antiferromagnetic (AFM) configuration (where all spins either point in or out of the center of the tetrahedron) is the ground magnetic state in $\text{Cd}_2\text{Os}_2\text{O}_7$ (Fig. 2), which is in agreement with previous studies [3,5,6,14,19,21,23].

We found that the GGA+SO approximation produces a metallic ground state in $\text{Cd}_2\text{Os}_2\text{O}_7$ (see the upper panel of Fig. 3), in contradiction with resistivity and optical measurements [1,2,12,15], which claim that $\text{Cd}_2\text{Os}_2\text{O}_7$ is an insulator. To produce the insulating magnetic ground state one has to take into account Coulomb electron correlations. The lower panel of Fig. 3 presents the energy band structure

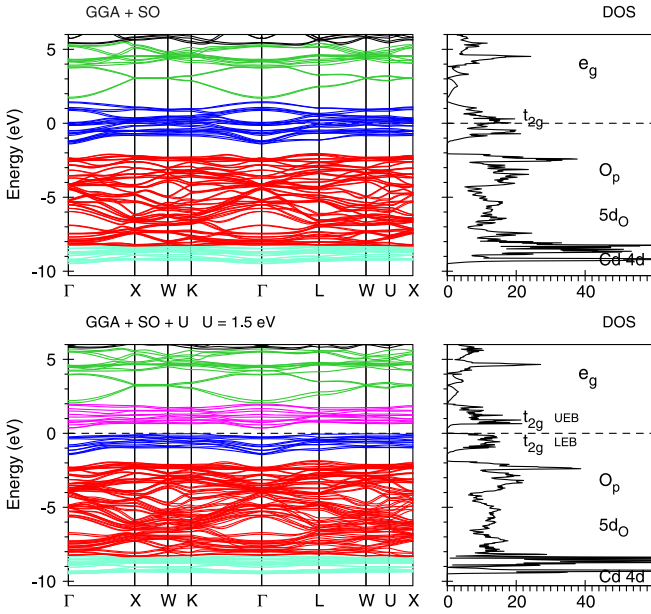


FIG. 3. The energy band structure and total DOSs of $\text{Cd}_2\text{Os}_2\text{O}_7$ calculated for the AIAO magnetic configuration in the GGA+SO (the upper panel) and GGA+SO+ U , $U_{\text{eff}} = 1.5$ eV (the lower panel) approximations.

of $\text{Cd}_2\text{Os}_2\text{O}_7$ calculated in the GGA+SO+ U approximation with $U_{\text{eff}} = 1.5$ eV.

The optical conductivity σ_{1xx} spectrum of $\text{Cd}_2\text{Os}_2\text{O}_7$ [Fig. 4(a)] displays a broad peak near 0.7 eV [15]. We adjusted U_{eff} to match the position of the dominant peak near 0.7 eV in the experimentally measured optical conductivity $\sigma_{1xx}(\omega)$ spectrum. The best agreement between the theoretically calculated and experimental optical conductivity is achieved with $U_{\text{eff}} = 1.5$ eV. Smaller values of U_{eff} overestimate the optical conductivity at 0.7 eV and underestimate it at 2 eV. Larger values of U_{eff} shift the theoretical spectrum toward higher energies. The GGA+SO approach produces the metallic ground state and, hence, noncorrect asymptotic behavior ($\omega \rightarrow 0$) for the optical reflectivity spectrum (the black dotted curve in the upper panel of Fig. 4).

Table I presents the theoretically calculated Os spin M_s , orbital M_l , and total M_{tot} magnetic moments in $\text{Cd}_2\text{Os}_2\text{O}_7$ as well as the theoretical direct and indirect energy gaps. Our GGA+SO+ U calculations produce an insulator solution in $\text{Cd}_2\text{Os}_2\text{O}_7$ in agreement with the experimental data but overestimate the direct gap and indirect gaps for $U_{\text{eff}} > 0.1$ eV in comparison with the optical measurements [15]. The orbital moment has to be quenched in the t_{2g}^3 state because there is only one possible orbital configuration with three spins aligned. However, there is still a small orbital moment at the Os site due to the strong Os $5d$ -O $2p$ hybridization. The spin and orbital angular momenta possess antiparallel coupling; this result appears compatible with Hund's third rule because the $5d^3$ system is less than half-filled. The total magnetic moment M_{tot} is equal to $1.244 \mu_B/\text{Os}$. This value is significantly smaller than the expected value of $3 \mu_B/\text{Os}$ for the $S = 3/2$ system; however, it is larger than the experimental value of $0.59 \mu_B/\text{Os}$ provided by Calder *et al.* [5] from NPD measurements. Shinaoka *et al.* [19] obtained theoretically

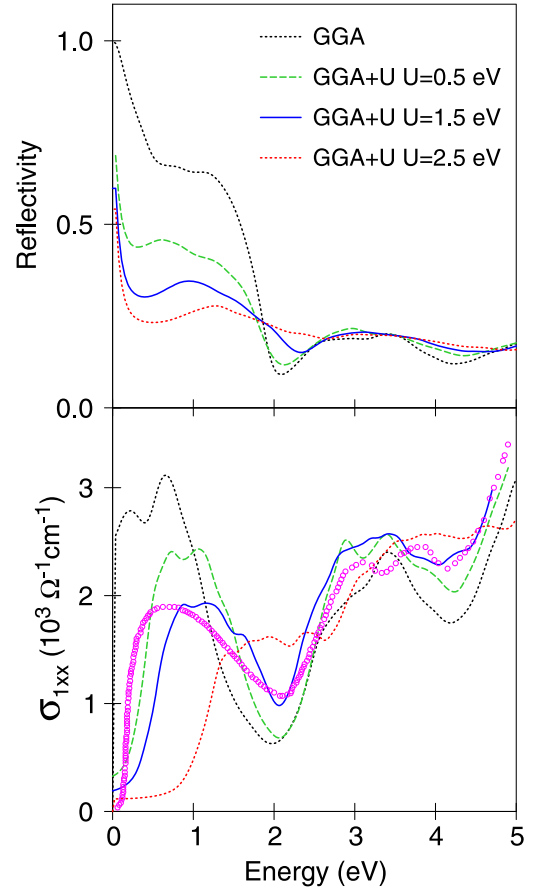


FIG. 4. Lower panel: The experimentally measured real part of the optical conductivity (open magenta circles), σ_{1xx} [15] (in $10^3 \Omega^{-1} \text{cm}^{-1}$), in $\text{Cd}_2\text{Os}_2\text{O}_7$ compared with the theoretical spectra calculated in the GGA+SO (the black dotted curve), and GGA+SO+ U with $U_{\text{eff}} = 0.5$ eV (the dashed green curve), $U_{\text{eff}} = 1.5$ eV (the full blue curve), and $U_{\text{eff}} = 2.5$ eV (the dotted red curve) approximations; the upper panel shows the theoretically calculated reflectivity spectra.

$M_s = 0.8$ – $1.1 \mu_B/\text{Os}$. In the experimental study by Yamauchi and Takigawa the net Os moment was estimated to be $\sim 1 \mu_B$ (see Ref. [16] in Ref. [14]). The reduction of magnetic moments has been noted in several systems with the $5d^3$

TABLE I. The theoretically calculated Os spin M_s , orbital M_l , and total M_{tot} magnetic moments (in μ_B) in $\text{Cd}_2\text{Os}_2\text{O}_7$ as well as the theoretical direct (ΔE_{dir}) and indirect (ΔE_{indir}) energy gaps (in eV) calculated for the AIAO magnetic ordering. The experimental direct optical gap and indirect, i.e., charge, gap are equal to 0.158 and 0.080 eV, respectively [15].

U_{eff} (eV)	Magnetic moments (μ_B)			Energy gap (eV)	
	M_s	M_l	M_{tot}	ΔE_{dir}	ΔE_{indir}
0.0	1.304	−0.060	1.244	0.245	0.052
0.1	1.348	−0.063	1.285	0.283	0.080
0.2	1.390	−0.066	1.324	0.323	0.109
0.5	1.505	−0.077	1.428	0.444	0.196
1.0	1.595	−0.058	1.537	0.563	0.404
1.5	1.661	−0.098	1.563	0.608	0.361

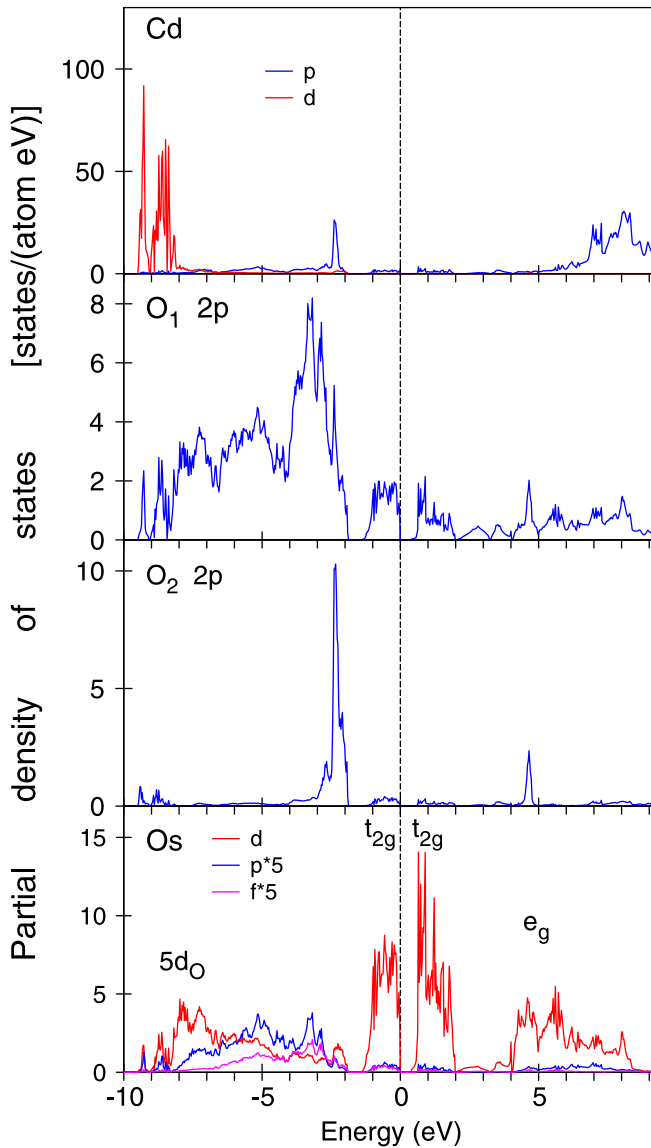


FIG. 5. The Os $5d$, Cd $4d$, and oxygen $2p$ partial DOSs for $\text{Cd}_2\text{Os}_2\text{O}_7$ with the AIAO magnetic configuration calculated in the GGA+SO+ U approximation with $U_{\text{eff}} = 1.5$ eV.

occupancy [31] and is often explained in terms of the extended orbitals in $5d$ systems and strong $5d$ – O $2p$ hybridization [5]. The magnetic moments as well as the energy gaps increase with increasing Hubbard U (see Table I).

Figure 5 presents the partial DOSs of $\text{Cd}_2\text{Os}_2\text{O}_7$ calculated in the GGA+SO+ U approximation with $U_{\text{eff}} = 1.5$ eV. Almost fully occupied Cd $4d$ states are situated below Os $5d$ states from -9.8 eV to -8.8 eV. Each Os^{5+} ion in $\text{Cd}_2\text{Os}_2\text{O}_7$ surrounded by six O_1^{2-} ions has three valent $5d$ electrons. The octahedral crystal field splits the Os t_{2g} and e_g manifolds, so that three electrons occupy the t_{2g} low energy band (LEB) manifold from -1.4 eV to 0 eV. The t_{2g} upper energy band (UEB) occupies the energy range from 0.05 eV to 2.0 eV. The e_g states spread from 2.2 eV to 8 eV. There is quite large $5d$ partial DOS in the energy interval from -8.8 eV to -1.9 eV due to the strong hybridization between Os $5d$ and oxygen $2p$ states. The occupation number of $5d$ electrons in the Os

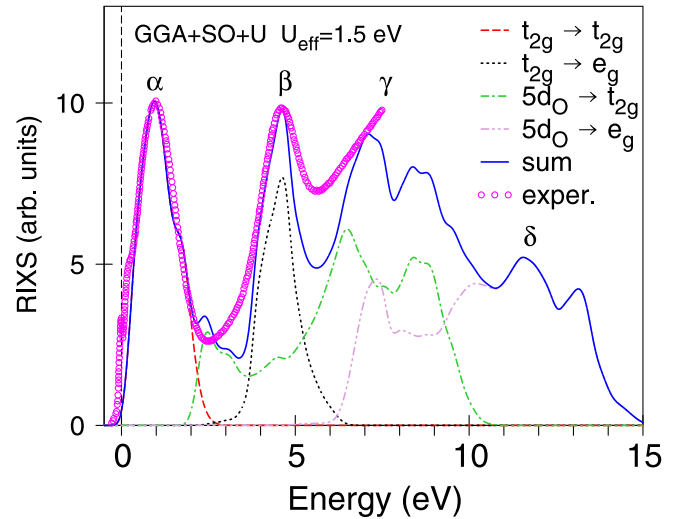


FIG. 6. The experimental RIXS spectrum (open magenta circles) at the Os L_3 edges for $\text{Cd}_2\text{Os}_2\text{O}_7$ [5] compared with the theoretical spectra (the full blue line) and the partial contributions from different interband transitions calculated in the GGA+SO+ U approximation ($U_{\text{eff}} = 1.5$ eV) with taking into account the core-hole effect.

atomic sphere is equal to 5.08 which is much larger than the expected value of three t_{2g} electrons. The excessive charge is provided by the “tails” of oxygen $2p$ states. These $5d_{\text{O}}$ states located from -8.8 eV to -1.9 eV play an essential role in the RIXS spectrum at the Os L_3 edge (see Sec. IV). The oxygen $2p$ states at the O_1 site are located from -9.8 eV to -1.9 eV, from -1.4 eV to 0 eV, and from 0.05 eV to 8.0 eV. They hybridize with Cd $4d$ states from -9.8 eV to -8.8 eV and with Os $5d$ states in the vicinity of the Fermi level. The oxygen $2p$ states at the O_2 site possess a single narrow peak located from -3.1 eV to -1.9 eV. There are corresponding narrow peaks in the Os $5d$ and Cd $5p$ partial DOSs at the same energy which reflect O_2 $2p$ –Os $5d$ and Cd $5p$ hybridization.

IV. Os L_3 RIXS SPECTRA

The experimentally measured RIXS spectrum at the Os L_3 edge consists of the peak centered at zero energy loss which comprises the elastic line and other low-energy features such as phonons, magnons, etc., and three inelastic excitations centered at 0.9 eV, 4.5 eV, and between 5.5 eV and 10 eV (α , β , and γ peaks) [5]. In addition, a small resolution-limited feature is observed experimentally at 0.16 eV [5]. Our calculations also distinguish a high-energy peak δ at around 12 eV.

Figure 6 shows the experimental RIXS spectrum measured by Calder *et al.* [5] (open magenta circles) compared with the theoretical spectra calculated in the GGA+SO+ U approximation with $U_{\text{eff}} = 1.5$ eV and taking into account the core-hole effect. We also present the partial contributions from different interband transitions. The low-energy peak α corresponds to intra- t_{2g} transitions. This peak is sensitive to the value of the energy gap in $\text{Cd}_2\text{Os}_2\text{O}_7$ and the relative position of the t_{2g} LEB and UEB bands (Fig. 5).

We found that the excitation β located at 4.5 eV is due to $t_{2g} \rightarrow e_g$ transitions, and therefore it gives a direct measure of the crystal field splitting in $\text{Cd}_2\text{Os}_2\text{O}_7$. However, there

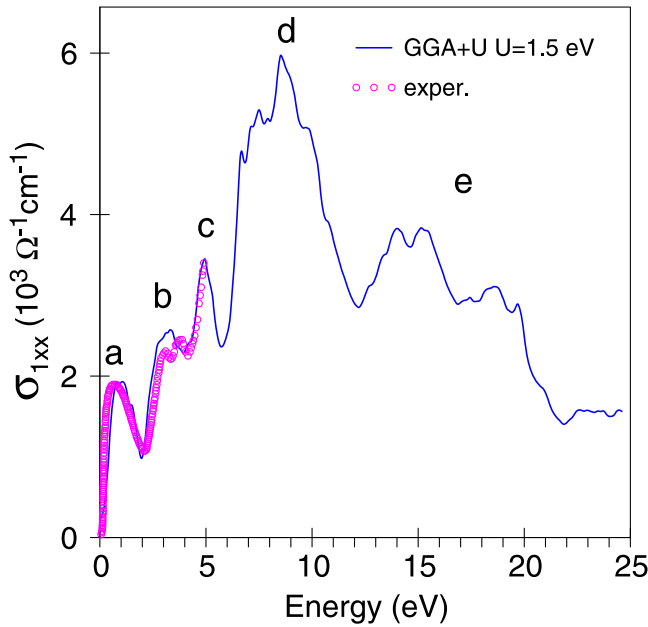


FIG. 7. The experimentally measured real part of the optical conductivity (open magenta circles), σ_{1xx} [15] (in $10^3 \Omega^{-1} \text{cm}^{-1}$), compared with the theoretical spectrum calculated in the GGA+SO+ U approximation with $U_{\text{eff}} = 1.5$ eV.

is a relatively large contribution to this peak also from the ligand-to-metal charge transfer excitations, d - d transitions to Os t_{2g} and e_g manifolds from the Os $5d_O$ states. The third wide structure γ situated from 5.5 eV to 10 eV is due to the $5d_O \rightarrow t_{2g}$ and some amount of $5d_O \rightarrow e_g$ transitions. The high-energy peak δ at 12 eV is fully due to $5d_O \rightarrow e_g$ transitions.

Our calculations were not able to reproduce the small low-energy peak at 0.16 eV. The energy of this excitation is smaller than the estimated direct energy gap and does not correspond to any expected d - d transitions. It requires careful interpretation beyond the one-particle approximation. Calder *et al.* [5] interpret this peak as the magnetic excitations corresponding to a superposition of multiple spin-flip processes.

It is interesting to compare the RIXS and optical spectra. Figure 7 presents the experimentally measured real part of the optical conductivity (open magenta circles), σ_{1xx} , [15] compared with the theoretical spectrum calculated in the GGA+SO+ U approximation ($U_{\text{eff}} = 1.5$ eV). Although the shape and energy position of the low-energy optical peak a coincide well with the corresponding α peak in the RIXS spectrum, these two spectra differ significantly from each other for higher energy.

RIXS and optical spectra have quite different nature. The α peak in the RIXS spectrum at the Os L_3 edge at around 0.9 eV can be assigned to a local excitations between the filled and empty t_{2g} states. More precisely, the incoming photon excites a $2p$ core electron into a t_{2g} UEB state what is followed by a deexcitation from the t_{2g} occupied LEB into the core level. The optical absorption is the interband transitions between occupied and empty valence bands. In optics, on-site d - d transitions are not allowed by the dipole selection rules. Therefore, the low-energy peak a in the optical absorption spectrum occurs from transitions between tails of p and f

character and d states at the Os site. They can be considered as intersite d - d transitions which change the number of d electrons similarly to the hopping. The peaks b and c in the optical absorption are due to interband transitions between oxygen $2p$ occupied states and the tails of the Os t_{2g} UEB state of d character in oxygen spheres. The low-energy shoulder of the peak b is almost completely defined by interband transitions from a narrow $2p$ peak located from -3.1 eV to -1.9 eV at the O_2 site (see Fig. 5). The high-energy shoulder of the peaks b and c is determined by the corresponding interband transitions at the O_1 site. The strong peak d at 7 – 13 eV in the optical absorption is due to transitions from oxygen $2p$ occupied states to the empty d oxygen states derived from the tails of Os e_g states at the oxygen sites as well as the interband transitions from Os p and f occupied states to the e_g states at the Os sites. The peak e situated between 14 eV and 24 eV occurs from the interband transitions between Cd $4d$ occupied and Cd $5p$ empty states. Such a structure is absent in the corresponding RIXS spectrum at the Os L_3 edge.

V. X-RAY ABSORPTION AND XMCD SPECTRA IN $\text{Cd}_2\text{Os}_2\text{O}_7$

Figure 8 presents the experimental x-ray absorption (the upper panels) and XMCD (the lower panels) spectra measured at 5 K under a 10 T magnetic field at the Os $L_{2,3}$ edges in $\text{Cd}_2\text{Os}_2\text{O}_7$ [18] in comparison with the theoretically calculated spectra in the GGA+SO+ U approximation with $U_{\text{eff}} = 1.5$ eV without (dashed red lines) and with (full blue lines) taking into account the core-hole effect.

The theoretically calculated Os $L_{2,3}$ XAS are in good agreement with the experiment. Our calculations show that the Os $L_{2,3}$ XAS are dominated by the empty e_g states with a small contribution from the empty t_{2g} orbitals at lower energy. The XMCD, however, mainly comes from the t_{2g} orbitals. This results in a shift between the XAS and XMCD maxima of the order of the cubic crystal field splitting Δ_{CF} . We found that the core-hole effect does not affect the XAS spectra but slightly improves the dichroism spectra at the Os $L_{2,3}$ edges.

VI. CONCLUSIONS

The electronic and magnetic structures of the pyrochlore $\text{Cd}_2\text{Os}_2\text{O}_7$ were investigated theoretically using first-principle calculations in the frame of the fully relativistic spin-polarized Dirac LMTO band-structure method in order to understand the importance of Coulomb interaction, spin-orbit coupling, and magnetic order in its temperature-induced and magnetic-related metal-insulator transition.

The SO coupling does not dominate the mechanisms creating the electronic ground state in $\text{Cd}_2\text{Os}_2\text{O}_7$, in contrast to $J_{\text{eff}} = 1/2$ Mott-like iridates. However, the intrinsically large SO coupling in $\text{Cd}_2\text{Os}_2\text{O}_7$ manifests itself in the stabilization of the AIAO magnetic ground state that was confirmed with neutron powder diffraction measurements [5].

The experimentally measured RIXS spectrum of $\text{Cd}_2\text{Os}_2\text{O}_7$ in addition to the elastic scattering peak at 0 eV possesses four inelastic excitations α , β , γ , and δ centered at 0.9 eV, 4.5 eV, between 5.5 eV and 10 eV, and at 12 eV, respectively. The low energy peak α corresponds to

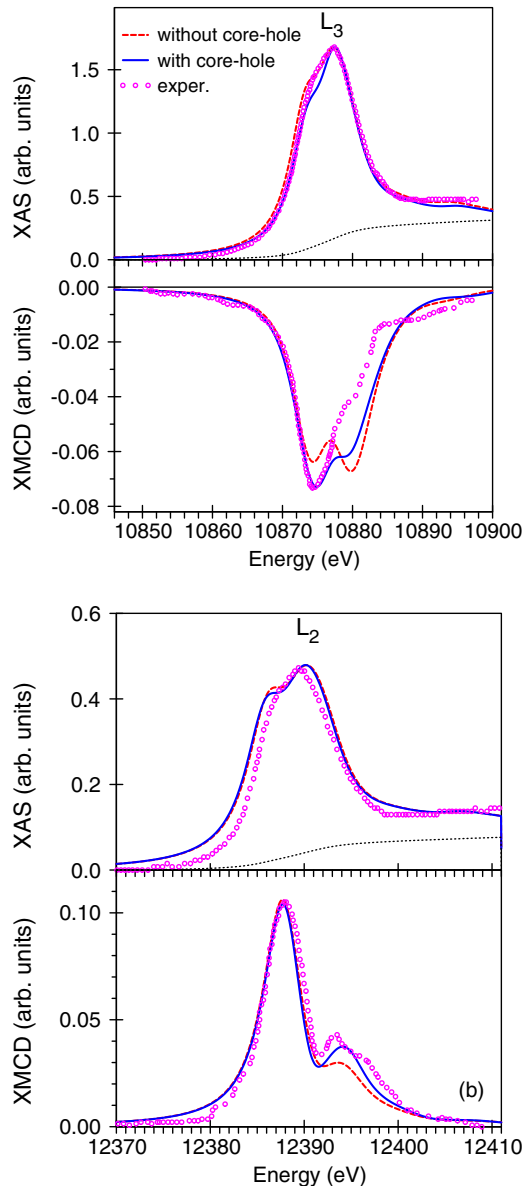


FIG. 8. The experimental x-ray absorption (the upper panels) and XMCD (the lower panels) spectra at the Os L_3 (a) and L_2 (b) edges in $\text{Cd}_2\text{Os}_2\text{O}_7$ (magenta circles) [18] measured at 5 K and an external magnetic field of 10 T compared with the theoretically calculated spectra in the GGA+SO+ U approximation with $U_{\text{eff}} = 1.5$ eV with (full blue curves) and without (dashed red blue curves) taking into account the core-hole effect. The dotted black curves in the upper panels show the background scattering intensity.

intra- t_{2g} transitions. The excitation β located at 4.5 eV is due to $t_{2g} \rightarrow e_g$ transitions with a significant contribution from $5d_0 \rightarrow t_{2g}$ transitions. The third wide structure γ situated from 5.5 eV to 10 eV is due to the ligand-to-metal charge transfer excitations $5d_0 \rightarrow t_{2g}$ and e_g . The high energy peak δ at 12 eV is fully due to $5d_0 \rightarrow e_g$ transitions. The GGA+SO+ U with $U_{\text{eff}} = 1.5$ eV calculations with taking into account the core-hole effect reproduce quite well the shape and the energy position of the α , β , and γ peaks.

RIXS and optical spectra have quite different nature. Although the shape and energy position of the low energy optical

peak a coincides well with the corresponding α peak in the RIXS spectrum, the spectra differ significantly from each other for higher energy due to different matrix elements. The RIXS spectrum at the Os L_3 edge can be assigned to local excitations between the filled and empty $5d$ states at the Os site. In optics, on-site $d-d$ transitions are not allowed by the dipole selection rules. Therefore, the optical absorption spectrum occurs from transitions between p , d and f states at each Os site in the unit cell.

The core-hole effect does not affect the XA spectra but slightly improves the dichroism spectra at the Os $L_{2,3}$ edges.

It is interesting to compare the electronic and magnetic structures as well as the RIXS spectra of NaOsO_3 presented in paper I [17] with the data for $\text{Cd}_2\text{Os}_2\text{O}_7$. There are some similarities and differences in these two osmates. NaOsO_3 is a G-type AFM Mott insulator which is characterized by AFM spins canted away from the c axis (the G-NCM configuration). The pyrochlore $\text{Cd}_2\text{Os}_2\text{O}_7$ possesses the frustrated AIAO magnetic ground state. Although two osmates possess quite different magnetic properties their energy band structures are very similar. Both the compounds have three valent $5d$ t_{2g} electrons in Os^{5+} ions. The Hubbard LEBs are separated from the HEBs by energy gaps. NaOsO_3 has a slightly larger direct energy gap in comparison with $\text{Cd}_2\text{Os}_2\text{O}_7$ (for the same value of U_{eff}). There is a significant amount of Os $5d$ DOS below the t_{2g} LEB in the region of the oxygen $2p$ bands in both the compounds which is mainly due to the “tails” of oxygen $2p$ electrons. As a result, the total $5d$ charge in the Os atomic sphere is much larger than the expected value of three t_{2g} electrons. These $5d_0$ states play an essential role in the RIXS spectrum at the Os L_3 edge. Due to a large crystal field splitting empty e_g states are high above the Fermi level spread from 2 eV to 8 eV in both the compounds.

Due to similarity in the band structures NaOsO_3 and $\text{Cd}_2\text{Os}_2\text{O}_7$ possess similar RIXS spectra with three inelastic excitations α , β , and γ . The low-energy peak α corresponds to intra- t_{2g} transitions. The excitation β is due to $t_{2g} \rightarrow e_g$ transitions and γ appears due to the ligand-to-metal charge transfer excitations. However, there are visible differences in the shape of the RIXS spectra in these osmates (compare Fig. 6 from Ref. [17] with Fig. 6 from this paper). The α and β peaks are relatively narrow with dip minimum in between in $\text{Cd}_2\text{Os}_2\text{O}_7$ in comparison with the wider peaks in NaOsO_3 with a less pronounced minimum between them. The details of γ peaks also differ from each other.

The core-hole effect is very important in the theoretical description of the RIXS spectra. This effect significantly reduces the value of the magnetic moments at the excited sites of both the osmates. It destroys the AFM ordering in NaOsO_3 (the compound becomes ferrimagnetically ordered). However, the AIAO magnetic ordering in $\text{Cd}_2\text{Os}_2\text{O}_7$ remains unchanged.

To reproduce the shape of the experimental RIXS spectra at the Os L_3 edge one has to take into account the Coulomb correlations with $U_{\text{eff}} = 1.5$ eV; therefore, both the osmates belong to Mott insulators.

ACKNOWLEDGMENTS

D.A.K. gratefully acknowledges the hospitality at the Max Planck Institute for Solid State Research in Stuttgart during

his stay there. The studies were supported by the National Academy of Sciences of Ukraine within the budget program

KPKBK 6541230 “Support for the development of priority areas of scientific research.”

-
- [1] A. Sleight, J. Gillson, J. Weiher, and W. Bindloss, *Solid State Commun.* **14**, 357 (1974).
- [2] D. Mandrus, J. R. Thompson, R. Gaal, L. Forro, J. C. Bryan, B. C. Chakoumakos, L. M. Woods, B. C. Sales, R. S. Fishman, and V. Keppens, *Phys. Rev. B* **63**, 195104 (2001).
- [3] J. Yamaura, K. Ohgushi, H. Ohsumi, T. Hasegawa, I. Yamauchi, K. Sugimoto, S. Takeshita, A. Tokuda, M. Takata, M. Udagawa, M. Takigawa *et al.*, *Phys. Rev. Lett.* **108**, 247205 (2012).
- [4] N. A. Bogdanov, R. Maurice, I. Rousochatzakis, J. van den Brink, and L. Hozoi, *Phys. Rev. Lett.* **110**, 127206 (2013).
- [5] S. Calder, J. Vale, N. Bogdanov, X. Liu, C. Donnerer, M. Upton, D. Casa, A. Said, M. Lumsden, Z. Zhao *et al.*, *Nat. Commun.* **7**, 11651 (2016).
- [6] J. G. Vale, S. Calder, N. A. Bogdanov, C. Donnerer, M. M. Sala, N. R. Davies, D. Mandrus, J. van den Brink, A. D. Christianson, and D. F. McMorrow, *Phys. Rev. B* **101**, 014441 (2020).
- [7] C. Donnerer, M. C. Rahn, M. M. Sala, J. G. Vale, D. Pincini, J. Stempfer, M. Krisch, D. Prabhakaran, A. T. Boothroyd, and D. F. McMorrow, *Phys. Rev. Lett.* **117**, 037201 (2016).
- [8] H. Guo, C. Ritter, and A. C. Komarek, *Phys. Rev. B* **94**, 161102(R) (2016).
- [9] V. N. Antonov, L. V. Bekenov, and D. A. Kukusta, *Phys. Rev. B* **102**, 195134 (2020).
- [10] Y. Wang, T. F. Rosenbaum, A. Palmer, Y. Ren, J.-W. Kim, D. Mandrus, and Y. Feng, *Nat. Commun.* **9**, 2953 (2018).
- [11] E. Buixaderas, S. Kamba, J. Petzelt, M. Savinov, and N. Kolpakova, *Eur. Phys. J. B* **19**, 9 (2001).
- [12] W. J. Padilla, D. Mandrus, and D. N. Basov, *Phys. Rev. B* **66**, 035120 (2002).
- [13] G. A. Thomas, D. H. Rapkine, S. A. Carter, A. J. Millis, T. F. Rosenbaum, P. Metcalf, and J. M. Honig, *Phys. Rev. Lett.* **73**, 1529 (1994).
- [14] Z. Hiroi, J. Yamaura, T. Hirose, I. Nagashima, and Y. Okamoto, *APL Mater.* **3**, 041501 (2015).
- [15] C. H. Sohn, H. Jeong, H. Jin, S. Kim, L. J. Sandilands, H. J. Park, K. W. Kim, S. J. Moon, D.-Y. Cho, J. Yamaura *et al.*, *Phys. Rev. Lett.* **115**, 266402 (2015).
- [16] I. Kwak, M.-C. Lee, B. C. Park, C. H. Kim, B. Lee, C. W. Seo, J. Yamaura, Z. Hiroi, T. W. Noh, and K. W. Kim, *Phys. Rev. B* **100**, 144309 (2019).
- [17] V. N. Antonov, D. A. Kukusta, and L. V. Bekenov, *Phys. Rev. B* **105**, 155144 (2022).
- [18] Y. H. Matsuda, J. L. Her, S. Michimura, T. Inami, M. Suzuki, N. Kawamura, M. Mizumaki, K. Kindo, J. Yamaura, and Z. Hiroi, *Phys. Rev. B* **84**, 174431 (2011).
- [19] H. Shinaoka, T. Miyake, and S. Ishibashi, *Phys. Rev. Lett.* **108**, 247204 (2012).
- [20] H. Harima, *J. Phys. Chem. Solids* **63**, 1035 (2002).
- [21] A. Uehara, H. Shinaoka, and Y. Motome, *Phys. Procedia* **75**, 495 (2015).
- [22] D. J. Singh, P. Blaha, K. Schwarz, and J. O. Sofo, *Phys. Rev. B* **65**, 155109 (2002).
- [23] G.-W. Chern and C. D. Batista, *Phys. Rev. Lett.* **107**, 186403 (2011).
- [24] M. A. Subramanian, G. Aravamudan, and G. V. S. Rao, *Prog. Solid State Chem.* **15**, 55 (1983).
- [25] J. P. Perdew, K. Burke, and M. Ernzerhof, *Phys. Rev. Lett.* **77**, 3865 (1996).
- [26] P. E. Blöchl, O. Jepsen, and O. K. Andersen, *Phys. Rev. B* **49**, 16223 (1994).
- [27] J. L. Campbell and T. Parr, *At. Data Nucl. Data Tables* **77**, 1 (2001).
- [28] A. Krajewska, T. Takayama, R. Dinnebier, A. Yaresko, K. Ishii, M. Isobe, and H. Takagi, *Phys. Rev. B* **101**, 121101(R) (2020).
- [29] O. V. Kovalev, H. T. Stokes, and D. M. Hatch, *Representations of the Crystallographic Space Groups*, 2nd ed. (Yverdon, Switzerland; Philadelphia, Pa., USA: Gordon and Breach, 1993).
- [30] A. S. Wills, M. E. Zhitomirsky, B. Canals, J. P. Sanchez, P. Bonville, P. D. de Reotier, and A. Yaouanc, *J. Phys.: Condens. Matter* **18**, L37 (2006).
- [31] A. E. Taylor, R. Morrow, D. J. Singh, S. Calder, M. D. Lumsden, P. M. Woodward, and A. D. Christianson, *Phys. Rev. B* **91**, 100406(R) (2015).